Elsevier Editorial System(tm) for Geochimica et Cosmochimica Acta
Manuscript Draft

Manuscript Number: GCA-D-15-00231

Title: Lower mantle hydrogen partitioning between periclase and perovskite: a quantum chemical modeling.

Article Type: Article

Corresponding Author: Prof. Alessandro Pavese,

Corresponding Author's Institution: University of Milan, Italy

First Author: Marcello Merli, Prof

Order of Authors: Marcello Merli, Prof; Costanza Bonadiman, Prof; Valeria Diella; Alessandro Pavese

Abstract: The partitioning of hydrogen (often addressed to as H2O) between periclase (pe) and perovskite (pvk) at lower mantle conditions (24-80 GPa) has been investigated, using quantum mechanics, equilibrium reaction thermodynamics and following two H-incorporation models. One is based on the replacements (MSWV) given by Mg2+↔2H+ and Si4+↔4H+; the other relies upon substitutions (MSWA) in terms of 2Mg2+↔Al3++H+ and Si4+↔Al3++H+. H2O partitioning between the two mentioned phases is considered in the light of homogeneous (Bulk Silicate Earth, BSE; pvk: 75% - pe:16% modal contents) and heterogeneous (Layered Mantle, LM; pvk:78% - pe:14% modal contents) mantle geochemical models, which are set up to bear lower and upper bulk H2O contents (BWC) of 800 and 1500 ppm, respectively. The equilibrium constant, [BWC]_K(P,T)_[D,H2O]^[pe/pvk], of the reactions governing the H-exchange between pe and pvk exhibits an almost negligible dependence on P, whereas it is remarkably sensitive to T, BWC and hydrogen incorporation scheme. Both MSWV and MSWA lead to [BWC]_K(P,T)_[D,H2O]^[pe/pvk] ≤1, which suggests an ubiquitous shift of the exchange reaction towards a H2O-hosting perovskite. This takes place more markedly in the latter model, thus showing that the H2O-partitioning is affected by the mechanism of uptake. In general, the larger BWC, the smaller is [BWC]_K(P,T)_[D,H2O]^[pe/pvk]. Over the BWC range of 800-1500 ppm, MSWV leads to a <[BWC]_K_[D,H2O]^[pe/pvk]> (average of [BWC]_K(P,T)_[D,H2O]^[pe/pvk] calculated along the lower mantle related P-T-paths predicted by the lower mantle geochemical models) that may be ultimately considered as a constant value (0.875). In the case of the MSWA mechanism, <[BWC]_K_[D,H2O]^[pe/pvk]> is more sensitive to BWC (and LM over BSE), but its values lie in the rather narrow range 0.610- 0.780. The concentration ratios (formally named "partition coefficient": CH2Ope/CH2Opvk) inferred from <[BWC]_K_[D,H2O]^[pe/pvk]> range, for MSWV, between 0.60 and 0.49 (BWC spanning from 500 to 3000 ppm). In this view, the MSWV partition coefficient is estimated to be 0.56. MSWA, in turn, yields a C_[H2O]^[pe]/C_[H2O]^[pvk]-trend having a slightly steeper negative slope (C_[H2O]^[pe]/C_[H2O]^[pvk] ratio: 0.6-0.3; BWC 500-3000 ppm), but over the interval 800-1500 ppm it may also be considered nearly invariant and as large as 0.47 (average over an interval between 0.43 and 051). Combining the results from MSWV and MSWA we propose that, in the P-T-BWC range of geochemical interest, the H2O pe/pvk "partition coefficient" lies in the short interval 0.47-0.56. This implies that water always prefers pvk than pe, but also suggests that even in a lower mantle with low or very low bulk water content, periclase hardly becomes a pure anhydrous phase.

Suggested Reviewers: Donato Belmonte Doc
resercher, Dipartimento di Scienze della terra, dell'ambiente e della vita, universirty of Genova, Italy

Donato.Belmonte@unige.it
modeling expert

William McDonough Prof
University of Maryland
mcdonoug@geol.umd.edu
geochemistry expert

William Griffin Prof
Macquarie University, Sidney
bill.griffin@mq.edu.au
geochemistry expert

David Price Prof
UCL; London's global university
d.price@ucl.ac.uk
modeling expert

Bernard Marty Prof
Centre de Recherches Pétrographiques et Géochimiques (CRPG), Vandœuvre les Nancy
bmarty@crpg.cnrs-nancy.fr
geochemistry expert

Dear Editor,

please, find enclosed the manuscript "**Lower mantle hydrogen partitioning between periclase and perovskite: a quantum chemical modeling"** by Macello Merli, Costanza Bonadiman, Valeria Diella and Alessandro Pavese for potential publication in Geochimica et Cosmochimica Acta..

The aim of the present work is to explore the partitioning of hydrogen (often addressed to as H_2O) between periclase and perovskite at lower mantle conditions (24-80 GPa), using quantum mechanics, equilibrium reaction thermodynamics and following two H-incorporation models. Subsequently we exploited the theoretical results to predict in the light of lower mantle geochemical models the hydration/dehydration trends and eventually the H_2O-distribution between *pe* and *pvk*.

We believe this work may be of interest to the readership of *Geochimica et Cosmochimica Acta*. This manuscript is an original work and has not been published, neither is it under consideration for publication elsewhere.

Thank you very much for your consideration and handling.

Milan 12/03/2015

Alessandro Pavese

Prof. Alessandro Pavese - Earth Sciences Department "Ardito Desio", University of Milan, Botticelli Street 23, 20133 Milan – Italy; Tel. +39 02 503 15603; fax. +39 02 503 15597; alessandro.pavese@unimi.it

Lower mantle hydrogen partitioning between periclase and perovskite: a quantum chemical modeling

Marcello Merli[a], Costanza Bonadiman[b], Valeria Diella[c], Alessandro Pavese[c,d,*]

[a] *Dipartimento di Scienze della terra e del Mare, Università degli Studi di Palermo, Via Archirafi 36, 90123 Palermo, Italy*

[b] *Dipartimento di Fisica e Scienze della terra, Università degli Studi di Ferrara, Via Saragat 1, 44122 Ferrara, Italy*

[c] *Consiglio Nazionale delle Ricerche, CNR-IDPA, Sezione di Milano, Via Botticelli 23, 20133 Milano, Italy*

[d] *Dipartimento Scienze della Terra "A. Desio", Università degli Studi di Milano, Via Botticelli 23, 20133 Milano, Italy*

Submitted to: *Geochimica et Cosmochimica Acta*

* Correspondence: Alessandro Pavese

fax:++39-02-503 15597

tel :++39-02-503 15603

e-mail: alessandro.pavese@unimi.it

key-words: H_2O-partitioning in lower mantle; *Ab-initio* calculations; periclase; perovskite.

Abstract

The partitioning of hydrogen (often addressed to as H_2O) between periclase (*pe*) and perovskite (*pvk*) at lower mantle conditions (24-80 GPa) has been investigated, using quantum mechanics, equilibrium reaction thermodynamics and following two H-incorporation models. One is based on the replacements (MSWV) given by $Mg^{2+} \leftrightarrow 2H^{+}$ and $Si^{4+} \leftrightarrow 4H^{+}$; the other relies upon substitutions (MSWA) in terms of $2Mg^{2+} \leftrightarrow Al^{3+}+H^{+}$ and $Si^{4+} \leftrightarrow Al^{3+}+H^{+}$. H_2O partitioning between the two mentioned phases is considered in the light of homogeneous (Bulk Silicate Earth, BSE; *pvk*: 75% - *pe*:16% modal contents) and heterogeneous (Layered Mantle, LM; *pvk*:78% - *pe*:14% modal contents) mantle geochemical models, which are set up to bear lower and upper bulk H_2O contents *(BWC*) of 800 and 1500 ppm, respectively. The equilibrium constant, ${}_{BWC}K(P,T)_{D,H_2O}^{pe/pvk}$, of the reactions governing the H-exchange between *pe* and *pvk* exhibits an almost negligible dependence on *P*, whereas it is remarkably sensitive to *T*, *BWC* and hydrogen incorporation scheme. Both MSWV and MSWA lead to ${}_{BWC}K(P,T)_{D,H_2O}^{pe/pvk} \leq 1$, which suggests an ubiquitous shift of the exchange reaction towards a H_2O-hosting perovskite. This takes place more markedly in the latter model, thus showing that the H_2O-partitioning is affected by the mechanism of uptake. In general, the larger *BWC*, the smaller is ${}_{BWC}K(P,T)_{D,H_2O}^{pe/pvk}$. Over the *BWC* range of 800-1500 ppm, MSWV leads to a $<{}_{BWC}K_{D,H2O}^{pe/pvk}>$ (average of ${}_{BWC}K(P,T)_{D,H2O}^{pe/pvk}$ calculated along the lower mantle related *P*-*T*-paths predicted by the lower mantle geochemical models) that may be ultimately considered as a constant value (0.875). In the case of the MSWA mechanism, $<{}_{BWC}K_{D,H_2O}^{pe/pvk}>$ is more sensitive to *BWC* (and LM over BSE), but its values lie in the rather narrow range 0.610-0.780. The concentration ratios (formally named "partition coefficient": $C_{H_2O}^{pe}/C_{H_2O}^{pvk}$) inferred from $<{}_{BWC}K_{D,H_2O}^{pe/pvk}>$ range, for MSWV, between 0.60 and 0.49 (*BWC* spanning from 500 to 3000 ppm). In this view, the MSWV partition coefficient is estimated to be 0.56. MSWA, in turn, yields a $C_{H_2O}^{pe}/C_{H_2O}^{pvk}$-trend having a slightly steeper negative slope ($C_{H_2O}^{pe}/C_{H_2O}^{pvk}$ ratio: 0.6-0.3; *BWC* 500-3000 ppm), but over the interval 800-1500 ppm it may also be considered nearly invariant and as large as 0.47 (average over an interval between 0.43 and 051). Combining the results from MSWV and MSWA we propose that, in the *P*-*T*-*BWC* range of geochemical interest, the H_2O $^{pe/pvk}$ "partition coefficient" lies in the short interval 0.47-0.56. This implies that water always prefers *pvk* than *pe*, but also suggests that even in a lower mantle with low or very low bulk water content, periclase hardly becomes a pure anhydrous phase.

1. INTRODUCTION

The mechanisms of hydrogen incorporation in nominally anhydrous minerals (NAM) govern the exchange of "water" (here we freely use such term, along with H_2O, to refer to the H-content of a mineral, expressed by oxides) between interior and surface of the Earth, as well as the degree of retention and possible abundance of hydrogen deep into our planet (Smyth, 2006; Johnson, 2006; Hirschmann 2006; Hirschmann and Kohlstedt 2012).

The exact water "budget" of the Earth's interior is currently unknown, but the availability constrains of the Earth geochemical models (McDonough and Sun, 1995; Wood and Corgne, 2007) suggest it to be comparable to the surface reservoirs'. Earth's core may contain water, after hints of metal-silicate partitioning experiments (Li and Agee, 1996; Abe et al., 2000; Saxena et al., 2004), although the volatile species geochemical model (Marty, 2012) does not support that H_2O could be stored there during the accretion and terrestrial differentiation processes.

Water mass estimates in the main mineral phases of our planet's interiors (i.e: Othani, 2005 and Murakami et al., 2002; Inoue et al., 2010), in combination with geochemical bulk models (i.e: McDonough and Sun, 1995; Lyubetskaya and Korenaga, 2007; Javoy et al., 2010), lead to that the Earth's mantle may host from about 0.5 to over 5 oceans at present-day (Huang et al. 2005; Smyth and Jacobsen 2006; Khan and Shankland , 2012; Marty, 2012).

The bulk silicate Earth chemical models yield that over 50% by weight of oxides are provided by MgO and FeO (e.g.: McDonough and Sun, 1995; Palme and O'Neill, 2003; Lyubetskaya and Korenaga, 2007; Javoy et al., 2010), with olivine (and its high-pressure β- and γ-polymorphs) as the dominant mineral of the upper mantle. Olivine, as most NAMs, incorporates hydrogen *via* intrinsic point defects of its structure (Ingrin and Skogby, 2000; Bolfan-Casanova, 2005; Hauri et al., 2006). This way, it accounts for an amount of water, in the upper 410 km of the mantle, nearly equivalent to the entire volume of the oceans (Hirschmann et al., 2005, 2009; Khan and Shankland, 2012).

The amount of water that NAMs can incorporate in the Transition Zone (410-660 km depth) is larger by as much as an order of magnitude (Bolfan-Casanova, 2005, Khan and Shankland, 2012) than that stored in the upper mantle (Hirschmann et al., 2005; Bonadiman et al., 2009; Inoue et al., 2010). Nominally anhydrous wadsleyite and ringwoodite in the lower part of the transition zone can accommodate up to 3.3 wt% water (Smyth, 1994; Bolfan-Casanova et al., 2000, Kleppe, 2006, Griffin et al., 2013). Over the volume of the Earth's transition zone, such phases represent a potential hydrogen reservoir that might store up to approximately four times the water present in the oceans and atmosphere (Hirschmann et al., 2006; Dai and Karato, 2009; Griffin et al., 2013).

In the lower mantle, the precise amount of stored water, its location and the mechanisms of exchange with the upper mantle are still a matter of debate (e.g. Hirschmann et al., 2005; Bolfan-Casanova et al., 2006; Panero et al., 2015). In such a region, Fe-periclase (~15% by volume) with a

composition of $Mg_{1-x}Fe_xO$, 0.1<x<0.2 (Ito and Takahashi, 1989; Ringwood, 1991; Guyot et al., 1988; Fiquet et al. 1998) and silicate Mg-perovskite (~80% by volume) are the principal mineral phases. Experimental studies (Bolfan-Casanova et al., 2000; Murakami et al., 2002; Litasov and Othani, 2007, Joachim et al., 2013) suggest that at 23-25 GPa and 1400-2000 ºC the partitioning coefficient for hydrogen between (Mg,Fe)O and (Mg,Fe)(Si,Al)O_3 is $\geq$1, with H_2O-contents in periclase ranging from 40-60 to 2000 ppm (Bolfan-Casanova et al., 2000; Murakami et al., 2002). However, Hernàndez et al. (2013) predict that in a Fe-free ambient water prefers to enter perovskite with respect to periclase, at 24 GPa and 1500 K. This all points to that, although extensive investigations (Mosenfelder et al., 2013; Jahn et al., 2013; Ghosh et al., 2013) have been devoted to hydrogen incorporation, yet much remains uncertain about the microscopic mechanisms underlying such reactions, in part because remarkable experimental difficulties make it complex to elucidate how the H_2O-partitioning takes place (Wood and Corgne, 2007). In literature, one finds out several models to account for the uptake of hydrogen in high-pressure mineral phases (Keppler and Bolfan-Casanova, 2006): cation-vacancy occurrence and introduction of H for compensation (hydro-garnet-like substitution); double replacement, such as 2Mg/1Si $\leftrightarrow$ Al(Fe^{3+})+H; reduction of iron to Fe-metallic (Litasov, 2010).

Although comparatively little is known about water solubility in periclase and perovskite at lower mantle pressure, the pure H_2O-MgO-SiO_2 system is probably a weak acceptor and most of the H-incorporation is related to double-replacement mechanisms involving mainly aluminum and iron (Litasov, 2010; Litasov and Othani, 2007; Bolfan-Casanova et al., 2006; Panero and Stixrude, 2004). As to Fe^{3+} in periclase, Demouchy et al. (2007) and Mackwell et al. (2005) discuss the role of ferric iron in combination with vacancy occurrence (at hydrous-ambient-pressure conditions), whereas Bolfan-Casanova et al. (2006) observe Fe anti-correlates with hydroxyl formation, at high pressure. In particular, Fe-periclase and perovskite can host hetero-valent cations through coupled substitutions as well as creation of point defects (Van Orman et al., 2009) over a wide *P*-*T* range. Fe^{3+} dwelling in (Mg,Fe)O (*i.e.* McCommon et al., 2004; Lin and Wheat, 2012; Otsuka et al., 2010) shows a pressure/oxygen fugacity dependence, so that in the lower mantle a change of the crystal-chemical behavior of ferric iron is expected (Otsuka et al., 2010). On the basis of experimental and theoretical data, it is plausible to assume that (Mg,Fe)O in the shallow part of the lower mantle ($P \approx$ 25-28 GPa) hosts Fe^{3+} in the octahedral sites, in combination with cation vacancies or occurrence of a monovalent cation (Na^+) to fulfill the charge balance (Mc Cammon et al., 2004). The solubility competition between monovalent cation (Na^+) and the protons (H^+) might play a role in affecting the tendency of H to site in periclase or pervoskite, and all this would ultimately affect the global evaluation of water content and transport properties, in the lower mantle.

In a simplistic “big picture”, the partition coefficients of moderately- and highly-siderophile elements between core-forming liquids and silicate melts determined at ambient pressure suggest

that such species should have entered almost entirely the Earth's core (McDonough and Arevalo, 2008). Seismological heterogeneities at the core-mantle boundary (*i.e*. 2300-2800 Km depth) reveal (Hilst et al., 1997 Lay et al. 1998; Nomura et al., 2014; Garnero et al. 2004) a distinct layer characterized by anomalous seismic velocities (Wysession et al., 1998), which have been interpreted by Kellogg et al. (1999) as due to a compositionally different and denser shell (D″). D″contains super-adiabatic thermal gradients in excess of 1000 K (Montelli et al., 2004; Wolfe et al., 2009) and is the region wherein mantle upwelling processes are supposed to have their rise. Changes in iron chemistry and Mg/Fe ratio due to phase transitions (Kellogg et al., 1999; Mao et al., 2006) could be responsible for such deep mantle layering. However, a potential segregation of even a small amount of water in this region, or in the Earth's core, could modify both melting relationships (e.g.: Inoue, 1994; Lay et al., 2004; Saxena et al.; 2004) and rheological properties (e.g.: Karato and Jung, 2003; Mei and Kohlstedt, 2000) drastically. The distribution of water has therefore an important influence on the dynamics and evolution, too, of terrestrial planets.

In this view, quantum mechanical modeling and computing techniques turn out to provide a valuable way to complement experimental issues, substantiating hypotheses or contributing to develop new ones. The aim of the present work is twofold: (1) using quantum mechanics [HF/DFT-LCAO calculations; CRYSTAL09-program (Dovesi et al., 2009)] we model the equilibrium constant, $K(P,T)_D$, for reactions involving an exchange of water between periclase (*pe*) and perovskite (*pvk*) at lower mantle regime, adopting two H-incorporation schemes; (2) we exploit the theoretical results to predict, in the light of lower mantle geochemical models, the hydration/dehydration trends and eventually the H_2O-distribution between *pe* and *pvk*.

2. GEOCHEMICAL CONSTRAINTS

H_2O partitioning between lower mantle phases depends on the potentially available water "budget" and, as a consequence, the Bulk Earth's geochemical model that accounts for the mantle chemical composition. We consider here two distinct lower mantle geochemical models:

1) homogeneous mantle model (BSE=Bulk Silicate Earth), which is inferred from the Primitive Upper Mantle (PUM) composition according to terrestrial data (pyrolite) and chondritic constraints (e.g.: Zindler and Hart, 1986; McDonough and Sun,1995; Lyubetskaya and Korenaga, 2007; Javoy et al., 2010), and it is extended to the whole silicate Earth;

2) heterogeneous mantle model (LM=layered mantle), which is based on geophysical data and cosmochemical constraints; it advocates a lower mantle chemically distinct from the upper mantle (e.g.: Stixrude and Bukowinski, 1992; Anderson, 1989; Cammarano and Romanowicz, 2007; Matas et al., 2007; Javoy et al., 2010). In particular, the lower mantle of LM bears a larger Si content (Mg/Si_{PUM} =1.21-1.31; Mg/Si_{LM} =1.18) than PUMS's in order to match the cosmochemical major

elements' contents of the bulk mantle (Matas et al., 2007).

The mineral phase compositions of the lower mantle, which are constrained by the geochemical model chosen, stem from mass balance calculations, aimed to give the best fit between supposed mineral phases and overall rock composition (Table 1). $CaSiO_3$-perovskite occurs along with (Mg,Fe)SiO_3-perovskite and (Mg,Fe)O-periclase. Although Al_2O_3 oxide accounts for about 3.5–4.5 wt% of the lower mantle, the aluminum host-phase is still uncertain. Al may reside in (Mg,Fe)O-*pe*, (Mg,Fe)SiO_3-*pvk* (Irifune 1994; Irifune et al. 1996), or form a separate Al-rich phase (Kesson et al., 1995; Oganov and Brodholt, 2000; Pamato et al., 2015). In Table 1, for the sake of simplicity, we assume Al_2O_3 as a "nondescript" H*P*-phase. Preliminary tests of mass balance have suggested us to exclude SiO_2-stishovite. The lower mantle H_2O content is here estimated by subtracting from the whole mantle (BM=bulk mantle) the contributions of the upper mantle and transition zone, normalized to their respective fractional masses (Table 2). Note that BM shares with BSE the H_2O content, excluding the surface water reservoirs (atmosphere, oceans and sedimentary rocks) and adopting a normalization to the total mass of the Earth, as proposed by Marty (2012).

H_2O global estimates converge to 250±50 ppm for the upper mantle (Dixon et al., 2002; Michael, 1988; Saal et al., 2002; Salters and Stracke, 2004) and 1.00±0.3 wt% for transition zone (Othani, 2005; Pearson et al., 2014). Using the conservative estimate of H_2O according to BSE, i.e. 1100- 3000 ppm (Palme and O'Neill, 2003; Othani, 2005; Marty, 2012), and combining it with the mantle mass factions, we infer the lower mantle's Bulk Water Contents (hereafter *BWC*) to range between a figure smaller than 1000 and 2000 ppm (Table 2), in agreement with earlier issues (Hernandez et al., 2013; Othani, 2005; Murakami et al., 2002). In this view, we have chosen to use 800 and 1500 ppm as reference average values for lower and upper estimates, respectively, of *BWC*, whose precise values depend on the geochemical model and will be considered below, in the Discussion, section 8.

3. H-INCORPORATION MODELING

Two mechanisms are here considered to account for H-incorporation in *pe* and *pvk*, at lower mantle conditions:

MSWV-scheme (Magnesium, Silicon, Water, Vacancies), relying upon

$$2\,H + V_{Mg} \leftrightarrow Mg \equiv H_2O \leftrightarrow MgO \quad (1.a)$$

$$4\,H + V_{Si} \leftrightarrow Si \equiv 2\,H_2O \leftrightarrow SiO_2, \quad (1.b)$$

and MSWA-scheme (Magnesium, Silicon, Water, Aluminum), based on

$$H + Al \leftrightarrow 2\,Mg \equiv Al_2O_3 + H_2O \leftrightarrow 4\,MgO \quad (2.a)$$

$$H + Al \leftrightarrow Si \equiv Al_2O_3 + H_2O \leftrightarrow 2\,SiO_2. \quad (2.b)$$

Other possible mechanisms of H-incorporation resorting to the introduction of Fe^{3+}, i.e.

$H + Fe^{3+} \leftrightarrow 2\ Mg \equiv Fe_2O_3 + H_2O \leftrightarrow 4\ MgO$

$H + Fe^{3+} \leftrightarrow Si \equiv Fe_2O_3 + H_2O \leftrightarrow 2\ SiO_2$,

are here neglected as we pay attention to partitioning reactions governed by sub-solidus atomic replacements, thus leaving out those that involve also REDOX-conditions of the environment. In equ.(1a-b), we assume an incorporation *via* replacement of one Mg/Si with 2/4 H atoms. Such a scheme leads to the formation of (i) hydroxyl groups (Smyth 2006), between entering H and coordination oxygens, and (ii) X-cation vacancies (V_X) at the expenses of either magnesium (in *pe*) or silicon (in *pvk*). In *pvk*, the substitution of one six-fold coordinated Si with four H atoms that establish as many hydroxyl groups with vertex oxygens of the same polyhedron accounts for a better capacity to accept and organize OHs in such a site, than in higher coordination ones (Williams and Hamley, 2001). In equ.(2a-b), H enters *pe* and *pvk* along with Al, to replace two Mg atoms and one Si atom, respectively. The sites vacated by Mg/Si host Al, whereas H establishes hydroxyls with coordination oxygens.

We base our leading reaction schemes on the equilibrium of a *x*-molar content of H_2O entering either *pe* (1 mole) or *pvk* (2 moles), in agreement with the phase molar proportions determined by the lower mantle models (Table 1). *x*-H_2O is often addressed to as "H/H_2O-uptake" or "H/H_2O-exchange". According to the MSWV scheme, the equation below holds

$$Mg_{1-x}O_{1-2x}(OH)_{2x}(pe\_x) + x\ MgO(pe) + 2\ MgSiO_3(pvk) \leftrightarrow$$
$$2\ MgSi_{1-x/4}O_{3-x/4}(OH)_{x/4}(pvk\_x) + (1-x/2)MgO(pe) + x/2\ MgSiO_3(pvk). \quad (3)$$

MSWA, which in turn is likely closer to the supposed physical uptake mechanism and requires an additional *x*-molar content of Al_2O_3, is associated to the equilibrium reaction shown beneath

$$(Mg_{1-4x}Al_{2x})O_{1-2x}(OH)_{2x}(pe\_x) + 4xMgO(pe) + 2\ MgSiO_3(pvk) \leftrightarrow$$
$$2\ Mg(Si_{1-x}Al_x)O_{3-x}(OH)_x(pvk\_x) + (1-2x)MgO(pe) + 2xMgSiO_3(pvk). \quad (4)$$

pe_x and *pvk_x* refer to H-bearing periclase and perovskite, with compositions according to the equations above. Note that we use a hydroxyl-based notation to stress the formation of OHs, as stated above.

4. EQULIBRIUM CONSTANT

At equilibrium, the reactions described by Equ.(3)-(4) require that

$$\Phi_{pe}\,\mu(pe) + \Phi_{pe\_x}\,\mu(pe\_x) + \Phi_{pek}\,\mu(pvk) = \Omega_{pe}\,\mu(pe) + \Omega_{pvk\_x}\,\mu(pvk\_x) + \Omega_{pvk}\,\mu(pvk) \quad (5.a)$$

or

$$\sum_k \Phi_k\,\mu(k) = \sum_j \Omega_j\,\mu(j) \quad (5.b)$$

where: $\mu(A)$ is the chemical potential associated to the *A*-component and depends on *P*,*T* and the system's composition. Moreover,

$$\mu(A) = \mu_0(A) + RT\, ln(a_A), \quad (5.c)$$

where: R is the gas constant, $\mu_0(A)$ depends on P and T only, and a_A is the activity. The equilibrium constant $K(P,T,x)_D$ for the reactions on study can be cast as

$$K(P,T,x)_D = \left[\frac{\prod_k a_k^{\Phi(k)}}{\prod_j a_j^{\Omega(j)}}\right] = \exp\left(-\Delta G_0(P,T,x)/RT\right), \quad (6.a)$$

where:

$$\Delta G_0(P,T,x) = \Phi_{pe\_x}\mu_0(pe\_x) - \Omega_{pvk\_x}\mu_0(pvk\_x) + (\Phi_{pe} - \Omega_{pe})\mu_0(pe) + (\Phi_{pvk} - \Omega_{pvk})\mu_0(pvk) \quad (6.b)$$

We have estimated the dependence of $\Delta G_0(P,T,x)$ on T *via* harmonic lattice dynamics modeling and semi-empirical potentials (Gale, 1997). At high-pressure regime we observe that the effect of the atomic vibrations dependent part of $\Delta G_0(P,T,x)$ is immaterial with respect to that due to the static contribution. Pressure, in turn, has been determined as $P=\partial E(V,T)/\partial V$, calculating by quantum-mechanics and semi-empirical potentials the static and vibrational energy contributions, respectively, for pure periclase and perovskite, only.

5. COMPUTING

A*b-initio* Linear-Combination-of-Atomic-Orbital calculations (HF/DFT-CRYSTAL09 program; Dovesi et al., 2009) have been carried out for *pe_x* and *pvk_x*, covering a pressure range from 24 to 80 GPa. The P range taken is so wide as to broadly encompass that of "pyrolite" liquidus (i.e.: Corgne et al., 2005) at lower mantle pressures inferred from melting experiments of Trønnes and Frost (2002) and Ito et al. (2004). At P > 24 GPa, the sub-solidus post-spinel transition is completed even in presence of 2 wt % H_2O (Ghosh et al., 2013), and setting an upper P-limit at 80 GPa (~ 2000 Km depth) allows one to exclude the D″ region, where the here chosen mineral portioning model cannot be used.

Periclase and perovskite structures have been relaxed to equilibrium at a given nominal pressure and 0 K, the former then corrected to account for thermal pressure. We have adopted a Hamiltonian based on the WC1LYP scheme (Scanavino et al., 2012; Scanavino and Prencipe, 2013), which contains a hybrid Hartree–Fock/density functional exchange-correlation term that mixes the WCGGA exchange component (Wu and Cohen, 2006) with the exact nonlocal HF exchange contribution and models correlation energy *via* the Lee-Yang-Parr GGA functional (Lee et al., 1988). In the case of *pe*, we have used a hybridization rate (HR) of 20%, whereas for *pvk* HR has been set at 28%. Such values have proven to model correctly equation of state, geometry and phase transition pressures [see Parisi et al. (2012)]. In order to assess the effect of energy-shift due to a different HR-ratios, we have sampled ten $H(P)$-values for perovskite, using a HR=20%, over the P-

277 interval here explored. The enthalpy differences, with respect to those by HR=28%, affect our main
278 issues (equilibrium constants and inferred concentration ratios) by 3 - 12%, a figure negligible in
279 view of the degree of approximation for so complex a process, and which does not cause any
280 significant shift of the equilibrium of the reactions (3) and (4). The following values have been used
281 for the tolerances governing the accuracy of the integrals of the self-consistent-field-cycles: 10^{-8} for
282 coulomb overlap, 10^{-8} for coulomb penetration, 10^{-8} for exchange overlap, 10^{-8} for exchange
283 pseudo-overlap in direct space and 10^{-12} for exchange pseudo-overlap in reciprocal space. A
284 threshold of 10^{-8} a.u. has been chosen for SCF-cycles' convergence, while, for the frequencies
285 calculation, the 10^{-10} threshold has been used. Anderson mixing model (Anderson, 1965) as a
286 convergence accelerator has been used. The reciprocal space has been sampled according to a
287 regular sub-lattice with a shrinking factor IS equal to 6 corresponding to 112 **k**-points through the
288 irreducible Brillouin zone for perovskie and 80 **k**-points for periclase. The convergence of the
289 geometry optimization process depends on the root-mean-square (RMS) and absolute value of the
290 largest component of both the gradients and nuclear displacements. The thresholds for the
291 maximum and the RMS forces (the maximum and the RMS atomic displacements) have been set at
292 0.00025 and 0.00020 a.u. and those for the maximum and the RMS atomic displacements at
293 0.00130 and 0.00100 a.u. Relaxation terminates when all four conditions are fulfilled. Dissolution
294 of water in *pe* and *pvk* has been modeled by super-cells (up to 64 and 125 octahedral sites, for MgO
295 and $MgSiO_3$, respectively) in which the replacements (1a-b) and (2a-b) mimic incorporation of H.
296 We tuned the super-cell's size in order to allow reproduction of different degrees of dilution of
297 water in the crystal structures, introducing one defect only at a time. For either incorporation
298 scheme, the positions of H and Al have been determined according a least-enthalpy principle,
299 exploring all possible H *versus* O configurations and taking into account the principle of local
300 charge balance. According to MSWV, the H atoms lie along one of the main diagonals of the
301 Si/Mg-emptied octahedron and establish hydroxyl groups with the oxygens at the ends; three
302 configurations in either mineral are possible. The MSWA-scheme leads to H atoms forming
303 hydroxyls with oxygens of the octahedron adjoining the one in which Al replaces Mg, in *pe*; the
304 involved oxygen atoms are second nearest neighbors of Al and the resulting OH-groups are slightly
305 canted from the main octahedral diagonal towards the aluminum-occupied site. The replacement of
306 Si with Al and introduction of H in *pvk* yields formation of a hydroxyl between hydrogen and an
307 oxygen of the octahedron hosting the cation substitution; six possible arrangements are possible.
308 The start Gaussian LCAO basis set of Mg was taken from Causà et al. (1986), then improved by the
309 addition of diffuse *sp* and *d* shells so as to obtain an 85-11G* contraction. For O, we used the basis
310 set of Ottonello et al. (2008) extended by a *d* shell to get an 84-11G* contraction. In the case of Fe,
311 the basis set of Valerio et al. (1995) was adopted, corresponding to an 86-41G* contraction scheme.
312 We also tried out a variational re-optimization of the exponents of the most diffuse Gaussian

functions of all the three elements, in *pe* and *pvk*, but without achieving any significant enhancement with respect to their original values. Further calculations have been carried out by semi-empirical potentials and lattice dynamics, using the GULP code, in order to estimate the effect of the vibration contribution on $\Delta G_0(P,T,x)$, as stated in the previous section. The Mg-O, Si-O, O-O interactions have been modelled by Buckingham-type potentials from the program's repository (Gale, 1997).

6. $K(P,T,x)_D$ CALCULATION

In the present instance, one has that

$$\mu_0(A\_x,P,T)=H_0(A\_x,P) - T\times S(A\_x)_{config}, \quad (7)$$

where $H_0(A\_x,P)$ and $S(A\_x)_{config}$ are enthalpy and configuration entropy of the *A_x* phase, taking into account that we restrict our energy calculations to static contributions, only. A first order expansion in *x* suffices to provide a correct descrtiption of the enthalpy as substantiated by the trends of $H_0(A\_x,P)$ for *pe_x* and *pvk_x* determined by exploring 80 *P-x* points systematically sampled over the interval 20-80 GPa, and 0-0.1, for either phase. Linear interpolations in *x* of points sharing the same *P* yield R-values larger than 0.999, so that $H_0(A\_x,P) \approx H_0(A,P) + \omega(A,P) \times x$, where ω depends on the incorporation scheme.

Altogether, equ.(6.b) for MSWV results in

$$\Delta G_0(P,T,x)=\{[\omega_{MSWV}(pe,P)-2\times\omega_{MSWV}(pvk,P)] + 0.5\times[3\times H_0(pe,P) - H_0(pvk,P)]\}\times x$$
$$-T\times\Delta S(x)_{MSWV,config} \quad (8.a)$$

and

$$\Delta S(x)_{MSWV,config} =R\times[x/2\times ln(4/3)+1/2\times x\times ln(x)+(1-x)\times ln(1-x)-2\times(1-x/4)\times ln(1-x/4)],$$

R being the gas constant in kJ/K.

For MSWA one has

$$\Delta G_0(P,T,x)=\{[\omega_{MSWA}(pe,P)-2\times\omega_{MSWA}(pvk,P)] + 2.0\times[3\times H_0(pe,P) - H_0(pvk,P)]\}\times x$$
$$- T\times\Delta S(x)_{MSWA,config} \quad (8.b)$$

and

$$\Delta S(x)_{MSWA,config} =R\times[2\times x\times ln(3/2)+(1-2\times x)\times ln(1-2\times x)-2\times(1-x)\times ln(1-x)].$$

Moreover, one observes that

$$\xi_{0,X}=3\times H_{0,X}(pe,P) - H_{0,X}(pvk,P) = a_{0,X} + a_{1,X}\times P + a_{2,X}\times P^2 \quad (9.a)$$

and

$$\xi_{\omega,X}=\omega_X(pe,P)-2\times\omega_X(pvk,P)= \omega_{0,X} + \omega_{1,X}\times P + \omega_{2,X}\times P^2, \quad (9.b)$$

so that

$$\Delta G_{0,X}(P,T,x)= (C\times\xi_{0,X}+\xi_{\omega,X})\times x- T\times\Delta S(x)_{X,config}= (\xi''_{0,X}+\xi_{\omega,X})\times x- T\times\Delta S(x)_{X,config}, \quad (10)$$

where: the subscript X stands for either MSWV or MSWA; C is set at 0.5,for MSWV, and at 2, for MSWA.

In Table 3 we set out the a_k/ω_j-parameters, referred to Equ.(9.a-b), which we have calculated for the MSVW and MSVA models. Note that if one assumes x-H_2O to be exchanged between partially hydrogenated perovskite and periclase, in contrast with the present model which relies on initially anhydrous H-exchangers, $K(P,T,x)_D$ would be just slightly affected with respect to the one from the calculations here reported.

7. RESULTS

Let us indicate, for the sake of brevity, by R(*pe_x*) and R(*pvk_x*) the left-hand and right-hand side member, respectively, of Equ.(3) and (4). A shift of the H-exchange reaction toward R(*pe_x*), or R(*pvk_x*), is here qualitatively associated to a "preference" of hydrogen to enter periclase, or perovskite, with respect to the other phase. In Figures 1a and b, we show isothermal $K(P,T,x)_D$ surfaces determined by either model using Equ.(6.a) at T=1500 and 2500 K (spanning the T-interval of geochemical interest), as a function of pressure and x. The latter ranges up to the largest H_2O-uptake compatible with 1 *pe* mole and 2 *pvk* moles, *i.e.* $x\approx0.02$, assuming a reference *BWC* of 1500 ppm. One observes that MSWV and MSWA lead to two different behaviors of the H_2O-partitioning mechanisms, though both models give $K(P,T,x)_D$ figures smaller than unity, thus suggesting a shift of the exchange reaction towards R(*pvk_x*). Such discrepancies are ascribable to the $(\xi''_0+\xi_\omega)$-functions of Equ.(10). In particular, one observes that: (i) $\xi''_0+\xi_\omega$ depends on P only, and $\Delta G_0(P,T,x)$ is weakly dependent on T *via* configuration entropy; (ii) MSWV and MSWA provide $(\xi''_0+\xi_\omega)$-figures ranging from 247 to 252, and from 774 and 942 kJ/mol, respectively, over the 10-80 GPa interval. We expect therefore MSWA to show a more marked sensitivity to temperature and pressure than MSWV. Figure 2 displays through the ξ_ω/ξ''_0-ratio an intrinsic difference between the two incorporation models. Note that that ξ_ω and ξ''_0 are reflective of the H-uptake mechanisms and "pure" *pe*/*pvk* behavior, respectively. In such a view, MSWV seems more prone to the cation substitution scheme than MSVA. Moreover, they exhibit ξ_ω/ξ''_0s having dissimilar trends as a function of P, which yet agree to display decreasing ξ_ω/ξ''_0-figures upon increasing pressure beyond 45 GPa.

MSWV and MSWA show a remarkable dependence on the H_2O-uptake, which leads to a general abatement of the equilibrium constant upon increasing x. By way of example, MSWV gives at 1500/2500 K and 80 GPa a $\Delta K(P,T,x)_D$, between 0 and 0.02, of 77/60%, against some 36/25% of MSWA. Temperature affects the $K(P,T,x)_D$ surface in terms of a shift towards unity at higher T-values. Such a behavior is consistent with that the larger T, the more the reaction model tends to

predict comparable penchants of *pe* and *pvk* to host hydrogen. "Low" *T*-values bring to light intrinsic differences between the incorporation mechanisms of MSWV and MSWA, yielding $K(P,T,x)_D$s that increasingly divert from one another. At x=0.02 and P=80 GPa, MSWV and MSWA lead to $\Delta K(P,T,x)_D$s, passing from 1500 to 2500 K, of 16 and 58%, respectively. At x=0.02 and T=1500/2500 K, MSWV and MSWA forecast changes of the equilibrium constant, from 24 to 80 GPa, of about 2-3 and 17-28%, respectively.

Altogether, all this points to an H-incorporation energetics dependent on the mechanism that accounts for the atomic replacements required to host hydrogen. Hence, other atomic substitution schemes might shed further light on how far such an uptake reaction is affected by the chemical species involved.

8. DISCUSSION

On the basis of some experimental studies, Fe-free periclase seems to accommodate almost no water into its structure (Bolfan-Casanova et al., 2000; 2002); conversely, other authors (Murakami et al., 2002; Litasov and Othani, 2007) assign to this phase a large capability of water incorporation, with H_2O-uptake ranging between 0.1 and 0.2 wt% (1000–2000 ppm). Such discrepancies might be reflective of the samples' compositions, of their being out of *P-T* thermodynamic equilibrium and/or of the analytical strategy for water measurement. The different techniques used , i.e. infra-red spectroscopy (Bolfan-Casanova et al., 2000; 2002) *versus* secondary ion mass spectroscopy (i.e: Inoue et al., 2010), may yield sets of values that are internally consistent but discrepant with each other (Hernandez et al., 2013).

The *BWC* is re-calculated for the *pe-pvk* system, in view of the chosen geochemical models. The Equ.(3) and (4) require slightly different lower/upper *BWC*-values of the lower mantle: BSE (MSWA, 865/1614 ppm): LM (MSWA, 854/1593 ppm); BSE (MSWV, 869/1629 ppm); LM (MSWV, 859/1608 ppm). Assuming that the temperature gradient of the lower mantle is mainly adiabatic, ∇T depends on the geochemical model and mineralogical composition (Turcotte and Schbert, 1982; Matas et al., 2007; Murakami et al., 2012). BSE and LM, which imply different mechanisms of convection, yield temperature gradients throughout the *P* range here investigated as large as 0.3 and 0.5 K/km, respectively, in agreement with Ono (2008); therefore, the ensuing *P-T* relationships we use are:

$$T(\mathrm{LM})=11.290\times P+1648 \qquad (11.a)$$

and

$$T(\mathrm{BSE})=6.596\times P+1686, \qquad (11.b)$$

P in GPa and *T* in K.

We introduce the notion of "average equilibrium constant", defined by the equation below

$$ {}_{BWC}K(P,T)_{D,H_2O}^{pe/pvk} = \frac{1}{BWC}\int_0^{BWC} K(P,T,x)_D \, dx \qquad (12) $$

where the integration is calculated over the possible H_2O-uptake values, i.e. *x* from 0.0, namely a fully anhydrous *pe+pvk* system, to *BWC* (≈0.01/0.02 molar fraction, according to Figs 1a-1b). For the sake of simplicity, we shall use the reference notations "1500" and "800" ppm to refer to maximum and minimum geochemically sound *BWC*, respectively, instead of its precise values actually adopted for calculations. One can then quantify the variations of the average equilibrium constant upon the *x*-range explored by means of

$$ \sigma_{BWC}K(P,T)_{D,H_2O}^{pe/pvk} = \sqrt{\frac{1}{BWC}\int_0^{BWC}[K(P,T,x)_D - {}_{BWC}K(P,T)_{D,H2O}^{pe/pvk}]^2 dx}. \qquad (13) $$

In some case, we express the average equilibrium constant in terms of ${}_{BWC}K(P,T)_{D,H_2O}^{pe/pvk}$ ($\pm\sigma_{BWC}K(P,T)_{D,H_2O}^{pe/pvk}$), where the figure between parentheses is meant to give a measure of the "dispersion" of ${}_{BWC}K(P,T)_{D,H_2O}^{pe/pvk}$, neither is it related to the conventional notion of experimental uncertainty.

The MSWV partitioning mechanism predicts (Fig. 3a) ${}_{BWC}K(P,T)_{D,H_2O}^{pe/pvk}$ decreasing upon increasing *BWC*, indicating a worsening of the H_2O-uptake capacity of *pe*, and a consequent shift of the exchange reaction towards *pvk*. Pressure is of weak import over the range explored, as proven by very close ${}_{BWC}K(P,T)_{D,H_2O}^{pe/pvk}$ values at 24 GPa and 80 GPa, for both 800 and 1500 *BWC*; the most relevant effects are due to temperature. $\sigma_{BWC}K(P,T)_{D,H_2O}^{pe/pvk}/{}_{BWC}K(P,T)_{D,H_2O}^{pe/pvk} < 0.1$ suggests a moderate dispersion. The difference between BSE and LM, in terms of *pe versus pvk* modal contents (*pe*/*pvk* : 0.21 *vs* 0.18), is likely too small to bring to light differences in the *pv-pvk* H_2O-uptake capacity following the MSWV partitioning mechanism.

MSWA shows similar features (Fig. 3b), but the differences between isobaric-curves, and between *BWC*s, are more marked than MSWV's. The different BSE and LM *pe*/*pvk* modal proportions are here revealed, though they modestly influence the ${}_{BWC}K(P,T)_{D,H_2O}^{pe/pvk}$ values in the MSWA exchange mechanism. $\sigma_{BWC}K(P,T)_{D,H_2O}^{pe/pvk}/{}_{BWC}K(P,T)_{D,H_2O}^{pe/pvk} < 0.25$ is significantly larger than MSWV's, as a consequence of the more quickly changing average equilibrium constant provided by MSWA. Notwithstanding that, the general behavior of ${}_{BWC}K(P,T)_{D,H_2O}^{pe/pvk}$ is univocally determined, neither, in especial, is any inversion of the H-exchange reaction between *pe versus pvk* forecast to take place over the explored *P-T* interval.

In full, both MSWV and MSWA show weakly varying ${}_{BWC}K(P,T)_{D,H_2O}^{pe/pvk}$-figures over the *P-T* range of geochemical interest. The LM-model leads to an H-exchange equilibrium constant ranging over 0.836/0.906(±0.09/±0.05)-0.860/0.920(±0.07/±0.04), for MSWV and 1500/800 ppm, and over 0.623/0.772(±0.182/±0.120)-0.649/0.787(±0.174/±0.113), for MSWA and 1500/800 ppm. BSE, in

turn, gives ${}_{BWC}K(P,T)_{D,H_2O}^{pe/pvk}$s lying in the intervals 0.830/0.902(±0.090/±0.053)-0.842/0.910(±0.084/±0.049), for MSWV and 1500/800 ppm, and 0.614/0.762(±0.188/±0.125)-0.607/0.757(±0.190/±0.127), for MSWA and 1500/800 ppm.

In view of so narrow ranges, we have chosen to introduce the following quantity:

$$<{}_{BWC}K_{D,H_2O}^{pe/pvk}> = \frac{1}{\Delta P}\int_{P0}^{Pmax} BWC^{K(P,T(P))_{D,H2O}^{pe/pvk}}\, dP$$

where $<{}_{BWC}K_{D,H_2O}^{pe/pvk}>$ represents the average ${}_{BWC}K(P,T)_{D,H_2O}^{pe/pvk}$ calculated along the lower mantle's *P*-*T*-paths predicted by LM and BSE. We think that $<{}_{BWC}K_{D,H_2O}^{pe/pvk}>$, which is somewhat a grand-average equilibrium constant, may be effective to provide an overall description for the H-exchange reactions as a function of *BWC* only.

BSE and LM provide $<{}_{BWC}K_{D,H_2O}^{pe/pvk}>$s close to one another, for a given incorporation scheme and *BWC* value (Table 4). $<{}_{BWC}K_{D,H_2O}^{pe/pvk}>$ shows an increasing sensitivity to *BWC* and, foremost, H-exchange mechanism. On the basis of the $<{}_{BWC}K_{D,H_2O}^{pe/pvk}>$s in Table 4 one determines the $d<{}_{BWC}K_{D,H_2O}^{pe/pvk}>/d(BWC)$ slopes, which are weakly dependent on the geochemical model and significantly sensitive to the microscopic reaction mechanism, thus obtaining -0.00003, for MSWA, and -0.00001 ppm^{-1}, for MSWV.

Altogether, in the *P*-*T* interval of interest (≈ 24-80 GPa, 1800-2600 K) and taking a bulk water content over the range of 800-1500 ppm, the *pe*/*pvk* H-exchange equilibrium constant of the MSWV mechanism may be ultimately considered as a constant value, ≈0.875. Such a figure is determined as the mean of the $<{}_{BWC}K_{D,H_2O}^{pe/pvk}>$ values in Table 4 for LM and BSE. In the case of the MSWA mechanism, $<{}_{BWC}K_{D,H_2O}^{pe/pvk}>$ is more sensitive to *BWC* (and LM over BSE), but its values still lie in a rather narrow range, namely 0.610- 0.780.

Let us describe the system perovskite+periclase+H_2O as anhydrous-periclase+anhydrous-perovskite+H-bearing-periclase+H-bearing-perovskite, such that equilibrium be provided by a H-exchange according to the reactions (3) and (4); taking into account that the H_2O-content is comparatively very small and assuming activity coefficients equal to unity then

$${}_{BWC}K(P,T)_{D,H_2O}^{pe/pvk} \approx \left[\left(\frac{\lambda_{pvk}}{\lambda_{pvk\_H}}\right)^2\left(\frac{\lambda_{pe\_H}}{\lambda_{pe}}\right)\right]$$

where: λ_A is the fraction molar content related to the *A*-phase; *pvk_H* and *pe_H* refer to H-bearing perovskite and periclase, respectively. For the sake of simplicity, we hypothesize that fully anhydrous phases (if any exists in the whole Earth's mantle) occur in negligible amount, and therefore λ_{pvk_H} and λ_{pe_H} are the sole significant terms stemming from the equilibrium reactions. In this view, $\lambda_{pvk\_H} + \lambda_{pe\_H} = 1$, and the equation above simplifies into

$$ {}_{BWC}K(P,T)_{D,H_2O^{pe/pvk}} \approx \frac{\lambda_{pe\_H}}{\left(1-\lambda_{pe\_H}\right)^2} . \quad (14) $$

Using Equ.(14) and $<{}_{BWC}K_{D,H_2O}{}^{pe/pvk}>$-values, one can calculate the ratio between the H_2O-contents hosted by periclase and perovskite (i.e $C_{H_2O}{}^{pe}/C_{H_2O}{}^{pvk}$). $C_{H_2O}{}^{pe}/C_{H_2O}{}^{pvk}$, formally named "partition coefficient", is therefore a useful instrument to direct compare our results with experimental data.

Figure 4 displays the $C_{H_2O}{}^{pe}/C_{H_2O}{}^{pvk}$ trends as a function of *BWC*, determined for the LM and BSE models using the $<{}_{BWC}K_{D,H_2O}{}^{pe/pvk}>$s of Table 4. Irrespective of the geochemical model, MSWV and MSWA give the same concentration ratio over the two phases ($C_{H_2O}{}^{pe}/C_{H_2O}{}^{pvk} \approx 0.6$) at "from low to very low" bulk water contents (*BWC*<500 ppm). Upon increasing the potential bulk water contents, the $C_{H_2O}{}^{pe}/C_{H_2O}{}^{pvk}$ ratio decreases, exhibiting divergent trends as a function of the exchange mechanism (Fig.4). In particular, one observes that the MSWV-linear interpolation's slope is close to 0 ($C_{H_2O}{}^{pe}/C_{H_2O}{}^{pvk}$ = 0.60-0.49; *BWC* spanning from 500 to 3000 ppm). In this light, we suggest that the $C_{H_2O}{}^{pe}/C_{H_2O}{}^{pvk}$ ratio for the lower mantle may be taken as large as 0.56, implying that *pe* accommodates from 237 to 538 ppm.

MSWA, in turn, leads to a $C_{H_2O}{}^{pe}/C_{H_2O}{}^{pvk}$-trend having a slightly steeper negative slope, which yields $C_{H_2O}{}^{pe}/C_{H_2O}{}^{pvk}$ ratios of ≈ 0.3 for a potential (unrealistic?) bulk water contents of 3000 ppm. In the region of 800-1500 ppm the MSWA-$C_{H_2O}{}^{pe}/C_{H_2O}{}^{pvk}$ ratio may also be considered nearly invariant and as large as 0.47, obtained as the average over the interval between 0.43 and 051; this leads to *pe* hosting H_2O in terms of 480-230 ppm.

Combining the results of MSWV and MSWA, we propose that, over the *P-T-BWC* range of interest (≈ 24-80 GPa, 1800-2600 K, 800-1500 ppm) the $C_{H_2O}{}^{pe}/C_{H_2O}{}^{pvk}$ ratio lies in the short interval of 0.47-0.56. Our results agree with those of Hernandez et al. (2013), insofar as H_2O prefers *pvk* over *pe*, but are at variance on the partition coefficient, which is predicted of 0.01 by the quoted authors, *versus* ours that is by one order of magnitude larger (0.47-0.56). Then, the present issues suggest that even in a lower mantle with low or very low bulk water content, periclase hardly becomes a pure anhydrous phase.

9. CONCLUSIONS

On the basis of two different H-incorporation mechanisms and two geochemical lower mantle models, the ${}_{BWC}K(P,T)_{D,H_2O}{}^{pe/pvk}$ values here calculated lie over the range from ≈0.6 to ≈0.9, showing that the H-exchange reactions shifts towards *pvk*, independently of the microscopic H-uptake scheme, i.e. MSWV, or MSWA. However, the H-incorporation models, MSWV and MSWA, lead

to dissimilar trends, the latter giving smaller equilibrium constant values and showing a more marked sensitivity to *P*-*T* than the former does. Both microscopic models give ${}_{BWC}K(P,T)_{D,H_2O}^{pe/pvk}$s that decrease upon augmenting the bulk water contents *(BWC)*, suggesting an increase of penchant of *pvk* to host water. In general, MSWV and MSWA exhibit a modest, quasi-negligible, dependence on *P*, whereas they are sensitive to temperature and foremost *BWC*. Note that ${}_{BWC}K(P,T)_{D,H_2O}^{pe/pvk}$ varies little over the *P*-*T* range predicted by the LM and BSE geochemical frames for the lower mantle, and can therefore be replaced by its average, $<{}_{BWC}K_{D,H_2O}^{pe/pvk}>$, calculated over the pressure-temperature path forecast by the geochemical models. Regardless of the microscopic H-exchange reaction, the LM and BSE models lead to $<{}_{BWC}K_{D,H_2O}^{pe/pvk}>$s ranging from 0.613 to 0.908, and from 0.589 to 0.899 respectively.

In full, the equilibrium constant of the H-incorporation reactions exhibits a complex dependence on both natural environment's variables (*P*, *T*, *BWC*) and microscopic mechanisms involved. If *pe* and *pvk* are supposed to occur in the lower mantle as H-bearing phases, then H_2O is distributed according to various possible partitioning mechanisms, of which we have here explored MSWV and MSWA, only. MSWV and MSWA lead to different K_D-values, whose discrepancies become apparent, in particular, if one takes $K(P,T,x)_D$. This suggests that the microscopic uptake scheme heftily affects the equilibrium constant. The experimentally determined H_2O contents in *pe* range from <10 ppm (Bolfan-Casanova et al., 2000; 2002), to 0.1-0.2 wt% (1000–2000 ppm; Murakami et al., 2002). Such discrepancies might be reflective of the following aspects: (i) partial thermodynamic equilibrium in experiments, with respect to the ideals of calculations; (ii) in view of the point above, defects (cation replacements and deviations from ideal crystal structure), which widely occur in specimens from a H*P*-H*T* synthesis, remarkably change the capacity of hosting hydrogen in a phase.

We therefore propose that, combining the results of MSWV and MSWA in the *P*-*T*-*BWC* range of interest (≈ 24-80 GPa, 1800-2600 K, 800-1500 ppm), the $C_{H_2O}^{pe}/C_{H_2O}^{pvk}$ ratio (commonly named "partition coefficient") lies in the interval 0.47-0.56. This implies that water always prefers *pvk* than *pe*, but it also suggests that even in a lower mantle with low or very low bulk water content, periclase hardly becomes a pure anhydrous phase.

AKNOWLEDGES

This study was supported by MIUR-2010EARRRZ_003 Grant (A.P.) and PNRA_2013 B02.02 (C.B).

549 **REFERENCES**

550 Abe Y., Ohtani E., Okuchi T., Righter K. and Drake. M. (2000) Water in the early Earth. In *Origin*
551 *of the Earth and Moon* (eds. R.M. Canup and K. Righter). University of Arizona Press, Tucson.
552 pp 413-433.

553 Ahrens T. J. (1989) Water storage in the mantle. *Nature* **342**, 122-123.

554 Anderson D. G. (1965) Iterative procedures for nonlinear integral equations. *J. Assoc. Comput.*
555 *Mach.* **12**, 547-560.

556 Anderson D. L. (1989) Composition of the Earth. *Science* **243**, 367–370.

557 Bolfan-Casanova N. (2005) Water in the Earth's mantle. *Min. Mag.* **69**, 229-257.

558 Bolfan-Casanova N., Keppler H. and Rubie D. C. (2000) Partitioning of water between mantle
559 phases in the system $MgO–SiO_2$-H_2O up to 24 GPa: implications for the distribution of water in
560 the Earth's mantle. *Earth Planet. Sci. Lett.* **182**, 209-221.

561 Bolfan-Casanova N., Mackwell S., Keppler H., McCammon C. and Rubie, D. C. (2002). Pressure
562 dependence of H solubility in magnesiowüstite up to 25 GPa: implications for the storage of
563 water in the Earth's lower mantle. *Geophys. Res. Lett.* **29** (10), 1029–1032.

564 Bolfan-Casanova N., McCammon C. A. and Mackwell S. J (2006) Water in transition zone and
565 lower mantle minerals. In *Earth's Deep Water Cycle* (eds**.** S.D Jacobsen and S. Van Der Lee)
566 Geophysical Monograph Series, Vol 168 AGU. doi:10.1029/168GM06.

567 Bonadiman C., Hao Y., Coltorti M., Dallai L., Huang U. and Xia Q. (2009) Water contents of
568 pyroxenes in intraplate lithospheric mantle. *Eur. J. Mineral*. **21**, 637-647.

569 Cammarano F., Romanowicz B. (2007) Insights into the nature of the transition zone from
570 physically constrained inversion of long period seismic data. *PNAS-High Pressure Geoscience*
571 **104,** 9139-9144.

572 Causà M., Dovesi R., Pisani C. and Roetti C. (1986) Electronic structure and stability of different
573 crystal phases of magnesium oxide. *Phys Rev* B **33**, 1308–1316.

574 Corgne, A., Liebske C., Wood B. J., Rubie D. C. and Frost D. J. (2005) Silicate perovskite-melt
575 patitioning of trace elements and geochemical signature of a deep perovkitic reservoir. *Geochim.*

576 *Cosmochim. Acta* **69**, 485–496.
577 Dai L. and Karato S. (2009) Electrical conductivity of wadsleyite at high temperatures and high
578 pressures. *Earth Planet. Sci. Lett*. **287**, 277-283.
579 Demouchy S., Mackwell S. J. and Kohlstedt D. L. (2007) Influence of hydrogen on Fe–Mg
580 interdiffusion in (Mg,Fe)O and implications for Earth's lower mantle. *Contrib. Mineral. Petrol.*
581 **154**, 279–289.
582 Dixon, J. E., Leist L., Langmuir C. and Schilling, J. G. (2002). Recycled dehydrated lithosphere
583 observed in plume-influenced mid-ocean-ridge basalt. *Nature* **420**, 385-389.
584 Dovesi, R., Saunders V. R., Roetti C., Orlando R., Zicovich-Wilson C. M., Pascale F., Civalleri B.,
585 Doll K., Harrison N. M., Bush I. J., D'Arco P., and Llunell M. (2009) CRYSTAL09 User's
586 Manual (University of Torino, Italy).
587 Fiquet G., Andrault D., Dewaele A., Charpin T., Kunz M. and Haüsermann D. (1998) P–V–T
588 equation of state of $MgSiO_3$. *Phys Earth Planet Int.* **105**, 21–31.
589 Gale J.D. (1997) GULP: A computer program for the symmetry-adapted simulation of solids *J.*
590 *Chem. Soc., Faraday Trans*. **93**, 629-637.
591 Garnero E. J., Maupin V., Lay T., and Fouch M. J. (2004) Variable azimuthal anisotropy in Earth's
592 lowermost mantle. *Science* **306**, 259–261.
593 Ghosh S., Ohtani E., Litasov K. D., Suzuki A., Dobson D., Funakoshi K. (2013) Effect of water in
594 depleted mantle on post-spinel transition and implication for 660 km seismic discontinuity. *Earth*
595 *Planet. Sci. Lett.* **371**, 103-111.
596 Griffin J. M., Berry J.A, Frost D. J., Wimperis S. and Ashbrook S. E. (2013) Water in the Earth's
597 mantle: a solid-state NMR study of hydrous wadsleyite. *Chem. Sci.* **4,** 1523-1538.
598 Guyot F., Madon M., Peyronneau J. and Poirier J. P. (1988) X-ray microanalysis of high-
599 pressure/high-temperature phases synthesized from natural olivine in a diamond anvil cell. *Earth*
600 *Planet. Sci. Lett.* **90,** 52–64.
601 Hauri E. H., Gaetani G. A. and Green, T. H. (2006) Partitioning of water during melting of the
602 Earth's upper mantle at H2O-undersaturated conditions. *Earth Planet. Sci. Lett*. **248**, 715-734

603 Hernàndez E. R., Alfè D. and Brodholt J. (2013) The incorporation of water into lower-mantle
604 perovskites:A first-principles study. *Earth Planet. Sci. Lett.* **364**, 37–43.
605 Hilst, R.D. van der, Widiyantoro, S., and Engdahl, E. R. (1997) Evidence for deep mantle
606 circulation from global tomography. *Nature* **386,** 578-584.
607 Hirschmann M. M. (2006). Water, melting, and the deep Earth H2O cycle. *Ann. Rev. Earth Planet.*
608 *Sci.* **34**, 629-653. doi:10.1146/annurev.earth.34.031405.125211.
609 Hirschmann M. M. and Kohlstedt D. (2012) Water in Earth's mantle. *Physics Today* **65**(3), 40-45.
610 Hirschmann M.M., Aubaud C. and Withers A.C. (2005). Storage capacity of H_2O in nominally
611 anhydrous minerals in the upper mantle. *Earth Planet. Sci. Lett.* **236,** 167-181
612 Hirschmann M. M., Tenner T., Aubaud C. and Withers, A. C. (2009) Dehydration melting of
613 nominally anhydrous mantle: The primacy of partitioning. *Phys Earth Planet Int.* **176**, 54-68.
614 Huang X., Xu Y. and Karato S. (2005), Water content in the transition zone from electrical
615 conductivity of wadsleyite and ringwoodite. *Nature* **434**, 746–749.
616 Ingrin J. and Skogby H. (2000) Hydrogen in nominally anhydrous upper mantle minerals:
617 Concentration levels and implications. *Eur. J. Mineral*. **12**, 543-570.
618 Inoue T. (1994) Effect of water on melting phase relations and melt composition in the system
619 Mg_2SiO_4-$MgSiO_3$-H_2O up to 15 GPa. *Phys*. *Earth Planet*. *Inter*. **85,** 237-263.
620 Inoue T., Wada T., Sasaki R. and Yurimoto, H. 2010. Water partitioning in the Earth's mantle. *Phys*
621 *Earth Planet Int*. **183**, 245–251.
622 Irifune T. (1994) Absence of an aluminous phase in the upper part of the Earth's lower mantle.
623 *Nature* **370**, 131-133.
624 Irifune T, Koizumi T and Ando J (1996) An experimental study of the garnet-perovskite
625 transformation in the system $MgSiO_3$–$Mg_3Al_2Si_3O_{12}$. *Geoph. Res. Lett.* **96**, 147–157.
626 Ito E. and Takahashi E. (1989). Postspinel transformations in the system Mg_2SiO_4–Fe_2SiO_4 and
627 some geophysical implications. *J. Geophys. Res*. **94**, Issue B8, 10637.
628 Ito E., Kubo A., Katsura T. and Walter M. J (2004) Melting experiments of mantle materials under
629 lower mantle conditions with implications for magma ocean differentiation. *Phys Earth Planet*

630 *Int.* **143-144**, 397-406.
631 Jahn S., Rahner R., Dachs E., Mrosko M. and Koch-Müller M. (2013) Thermodynamic properties
632 of anhydrous and hydrous wadsleyite, β−Mg_2SiO_4. *High Pressure Res.* **33,** 584-594.
633 Javoy M., Kaminski E., Guyot F., Andrault D., Sanlou J. R., Moreira M., Labrosse S., Jambon A.,
634 Agrinier P., Davaille A. and Jaupart C.(2010) The chemical composition of the Earth: Enstatite
635 chondrite models. *Earth Planet. Sci. Lett*. **293**, 259-268.
636 Joachim B., Wohlers A., Norberg N., Garde´s E., Petrishcheva E. and Abart R. (2013) Diffusion
637 and solubility of hydrogen and water in periclase. *Phys Chem Minerals* **40,** 19–27.
638 Johnson E. A. (2006) Water in nominally anhydrous crustal minerals: speciation, concentration and
639 geological significance. In *Reviews in Mineralogy and Geochemistry* (eds. J. Smyth and H.
640 Keppler), Mineralogical Society of America, Vol. 62, 117-154.
641 Karato S. and Jung H. (2003) Effects of pressure on high-temperature dislocation creep in olivine
642 polycrystals. *Philos. Mag. A* **83**, 401–414.
643 Kellogg L. H., Hager B. H., and Hilst R. D. van der (1999) Compositional stratification in the deep
644 mantle. *Science* **283**, 1881–1884.
645 Keppler H. and Bolfan-Casanova N. (2006) Thermodynamics of water solubility and partitioning.
646 In: Water in nominally anhydrous minerals. In *Reviews in Mineralogy and Geochemistry* (eds:
647 J.Smyth and H. Keppler), Mineralogical Society of America, **62**, 193-230.
648 Kesson S. E., Fitz Gerald J. D., Shelley, J. M. G. and Withers, R. L. (1995) Phase relations,
649 structure and crystal chemistry of some aluminous silicate perovskites. *Earth Planet. Sci. Lett*.
650 **134**, 187–201.
651 Khan A. and Shankland T. J. (2012) A geophysical perspective on mantle water content and
652 melting: Inverting electromagnetic sounding data using laboratory-based electrical conductivity
653 profiles. *Earth Planet. Sci. Lett*. **317-318**, 27–43.
654 Kleppe A. K. (2006) High-pressure Raman spectroscopic studies of hydrous wadsleyite II.
655 *Am.Mineral.* **91**, 1102–1109.
656 Lay T, Garnero E. J., Williams Q. (2004) Partial melting in a thermo-chemical boundary layer at the

base of the mantle. *Phys. Earth Planet. Inter.* **146**, 441-467.

Lay T., Williams Q. and Garnero, E. J. (1998) The core–mantle boundary layer and deep Earth dynamics. *Nature* **392**, 461–468.

Lee C., Yang W. and Parr R. G. (1988) Development of the Colle-Salvetti correlation-energy formula into a functional of the electron density. *Phys. Rev.* B **37**, 785–789.

Li J. and Agee C. B. (1996) Geochemistry of mantle–core differentiation at high pressure. *Nature* **381**, 686 - 689.

Lin J.F. and Wheat A. (2012). Electronic spin transition of iron in the Earth's lower mantle. *Hyperfine Interact.* **207**, 81-88.

Litasov K. D, Ohtani E., Langenhorst F., Yurimoto H., Kubo T. and Kondo, T. (2003). Water solubility in Mg-perovskites, and water storage capacity in the lower mantle. *Earth Planet. Sci. Lett*. **211**, 189-203.

Litasov K. D. (2010) The influence of Al_2O_3 on the H_2O content in periclase and ferropericlase at 25 GPa. *Russ. Geol. Geophys*. **51**, 644–649.

Litasov K. D. and Ohtani E. (2007). Effect of water on the phase relations in Earth's mantle and deep water cycle. In *Advances in High-pressure Mineralogy* (ed E. Ohtani, E.),. Geological Soc. Amer., pp.115-156.

Lyubetskaya T. and Korenaga J. (2007) Chemical composition of Earth's primitive mantle and its variance: 1. method and results. *J. Geophys. Res*. **112 (**B3**),** B03211, doi:10.1029/2005JB004223.

Mackwell S. J., Bystricky M. and Sproni C. (2005) Fe–Mg interdiffusion in (Mg,Fe)O. *Phys Chem Mineral*. **32**, 418–425.

Mao W. L., Mao H-k, Sturhahn W., Zhao J., Prakapenka V.B., Yue Meng Y., Shu J., Fei Y. and Hemley R. J. (2006) Iron-Rich Post-Perovskite and the Origin of Ultralow-Velocity Zones. *Science* **312**, 564-565.

Marty B. (2012) The origins and concentrations of water, carbon, nitrogen and noble gases on Earth. *Earth Planet. Sci. Lett.* **313–314**, 56–66.

Matas J., Bass J., Ricard Y., Mattern E. and. Bukowinski M. S. T. (2007) On the bulk composition of the lower mantle: predictions and limitations from generalized inversion of radial seismic profiles. *Geophys. J. Int.* **170,** 764–780.

McCommon C. E, Stachel T. and Harris J. W. (2004) Iron oxidation state in lower mantle mineral assemblages II. Inclusions in diamonds from Kankan, Guinea. *Earth Planet. Sci. Lett*. **222**, 423-434.

McDonough W. F and Arevalo R. (2008) Uncertainties in the composition of Earth, its core and silicate sphere**.** *J. of Phys -Conference Series* **136** 022006 (abstr)**.**

McDonough W. F. and Sun S. (1995) The composition of the Earth. *Chem. Geol*. **120**, 223–253.

Mei S. and Kohlstedt D. L. (2000) Influence of water on plastic deformation of olivine aggregates: 2. Dislocation creep regime. *J. Geophys. Res*. **105**, 21,471-21,481.

Michael P. J. (1988) The concentration, behavior and storage of H2O in the suboceanic upper mantle - Implications for mantle metasomatism. *Geochim. Cosmochim. Acta* **52**, 555-566.

Montelli R., Nolet G., Masters G., Engdahl E. R. and Hung S.-H. (2004) Finite-frequency tomography reveals a variety of plumes in the mantle. *Science*, **303,** 338- 343.

Mosenfelder J. L., Sharp T. G., Asimow P. D.and Rossman G. R. (2013) Hydrogen Incorporation in natural mantle olivines. In *Earth's Deep Water Cycle* (eds S. D. Jacobsen and S. Van Der Lee), American Geophysical Union, Washington, D. C.. doi: 10.1029/168GM05.

Murakami M., Ohishi Y., Hirao N. and Hirose K. (2012) A perovskitic lower mantle inferred from high-pressure, high-temperature sound velocity data. *Nature* **485**, 90-94.

Murakami M., Hirose K., Yurimoto H., Nakashima S. and Takafuji N. (2002) Water in Earth's lower mantle. *Science* **295**, 1885, doi:10.1126/science.1065998.

Nomura R., Hirose K., Uesugi K., Ohishi Y., Tsuchiyama A., Miyake A., and Ueno Y. (2014) Low core-mantle boundary temperature inferred from the solidus of pyrolite. *Science* **343**, 522–525.

Oganov, A. R. and Brodholt, J. P. (2000) High –pressure phases in the Al_2SiO_5 system: the problem of aluminous phase in the Earth's lower mantle: a*b initio* calculations. *Phys. Chem. Miner*. **27**, 430-439.

711 Ohtani E.(2005). Effect of water on phase transitions in the Earth's mantle. *Elements* **1**, 25–30.
712 Ono S. (2008) Experimental constraints on the temperature profile in the lower mantle. *Phys. Earth*
713 *and Planet. Inter*. **170**, 267–273.
714 Otsuka K., McCammon C. A. and Karato S-I (2010) Tetrahedral occupancy of ferric iron in
715 (Mg,Fe)O: Implications for point defects in the Earth's lower mantle. *Phys. Earth and Planet.*
716 *Inter*. **180**, 179-188.
717 Ottonello G., Civalleri B., Ganguly J., Vetuschi Zuccolini M. and Noel Y. (2008) Thermo-physical
718 properties of the a–b–c polymorphs of Mg_2SiO4: an all-electron ab initio study. *Phys. Chem.*
719 *Miner.* **36**, 87–106.
720 Palme H. and O'Neill H. St. C. (2004) Cosmochemical estimates of Mantle Composition. In:
721 *Treatise on Geochemistry (*eds , H.D Holland and K.K Turekian) Elsevier, Amsterdam, The
722 Netherlands, Vol.2, pp 1-38.
723 Pamato M. G., Myhill R, Boffa Ballaran T., Frost D. J., Heidelbach F. and Miyajima N. (2015)
724 Lower-mantle water reservoir implied by the extreme stability of a hydrous aluminosilicate.
725 *Nature Geoscience* **8**, 75–79.
726 Panero W. R. and Stixrude L. (2004) Hydrogen incorporation in stishovite at high pressure and
727 symmetric hydrogen bonding in d-AlOOH. *Earth Planet. Sci. Lett.* **221**, 421–431.
728 Panero W. R., Pigotti J. S.,. Reaman D. M, Kabbes J.E and Liu Z. (2015) Dry (Mg,Fe)SiO_3
729 perovskite in the Earth's lower mantle. *J. Geophys. Res. Solid Earth* **12** 0,
730 doi:10.1002/2014JB011397.
731 Parisi F., Sciascia L., Princivalle F. and Merli M. (2012) The pressure induced ringwoodite to Mg-
732 perovskite and periclase post-spinel phase transition: a Bader's topological analysis of the ab
733 initio electron densities. *Phys. Chem. Miner.* **39**, 103–113.
734 Pearson D.G., Brenker F. E., Nestola F., McNeill J., Nasdala L., Hutchinson M.T., Matveev S.,
735 Mather K., Slversmit G., Schmitz S., Vekemans B. and Vincze L. (2014) Hydrous mantle
736 transition zone indicated by ringwoodite included within diamond. *Nature* **507**, 221-224.
737 Ringwood A. E. (1991) Phase transitions and their bearing on the constitution and dynamics of the

738 mantle. *Geochim Cosmochim Acta* **55**, 2083–2110.
739 Saal A. E., Hauri E., Langmuir C. H. and Perfit M. R.(2002) Vapour undersaturation in primitive
740 mid-ocean-ridge basalt and the volatile content of Earth's upper mantle. *Nature* **419**, 451–455.
741 Salters V.J.M. and Stracke, A. (2004) Composition of the depleted mantle. *Geochem. Geophys.*
742 *Geosyst.* **5**, 27, DOI: 10.1029/2003GC000597.
743 Saxena S. K., Liermann H-P. and Shen G. (2004). Formation of iron hydride and high-magnetite at
744 high pressure and temperature *Phys. of the Earth and Planet. Int.* **146**, 313–317.
745 Scanavino I., Belousov R. and Prencipe M. (2012) Ab initio quantum-mechanical study of the
746 effects of the inclusion of iron on thermoelastic and thermodynamic properties of periclase
747 (MgO). *Phys. Chem. Miner.* **39**, 649–663.
748 Scanavino I. and Prencipe M. (2013) Ab-initio determination of high-pressure and high-temperature
749 thermoelastic and thermodynamic properties of low-spin (Mg1–xFex)O ferropericlase with x in
750 the range [0.06, 0.59]. *Am. Mineral.* **98**, 1270–1278.
751 Smyth J. R. (1994) A crystallographic model for hydrous wadsleyite: An ocean the Earth's interior?
752 *Am. Mineral.* **79**, 1021-1025.
753 Smyth J. R. (2006) Hydrogen in high pressure silicate and oxide mineral structures. In *Water in*
754 *nominally anhydrous minerals* (eds. J. Smyth and H. Keppler). Geochemical Society-
755 Mineralogical Society of America, Vol. 62 pp 85-115.
756 Smyth J. R. and Jacobsen S. D. (2006) Nominally anhydrous minerals and Earth's deep water cycle.
757 In *Earth's Deep Water Cycle* (eds. S.D. Jacobsen and S. van der Lee). American Geophysical
758 Union, Geophysical Monograph, Vol. 168 pp 1-11.
759 Stixrude L. and Bukowinski M. S. T. (1992) Stability of (Mg,Fe)SiO_3 perovskite and the structure
760 of the lowermost mantle. *Geoph. Res Lett.* **19**, 1057-1060.
761 Trønnes R. G. and Frost D. J. (2002) Peridotite melting and mineral-melt partitioning of major and
762 minor elements at 21-24 GPa. *Earth Planet. Sci. Lett*. **197**, 117-131.
763 Turcotte D. L. and Schubert G. (1982)Ge odynamics. Wiley, New York, pp. 456.
764 Valerio G., Catti M., Dovesi R. and Orlando R. (1995) Ab initio study of antiferromagnetic rutile-

765 type FeF2. *Phys Rev* B **52**, 2422–2427.
766 Van Orman J. A., Li C. and Crispin K. L. (2009) Aluminum diffusion and Al-vacancy association
767 in periclase. *Phys. Earth and Planet Int.* **172**, 34-42.
768 Walter, M. J., Kubo A., Brodholt J., Koga K. T., and Ohishi Y. (2004) Phase relations and equation-
769 of-state of aluminous Mg-silicate perovskite and implications for the Earth's lower mantle. *Earth*
770 *Planet. Sci. Lett.* 222, 501–516.
771 Williams Q. and Hamley R. J. (2001) Hydrogen in the deep Earth. *Annu. Rev. Earth Planet. Sci*. **29**,
772 365–418.
773 Wolfe, C. J., Solomon, S.C., Laske, G., Collins, J.A., Detrick, R. S., Orcutt, J. A., Bercovici D., and
774 Hauri, E. H. (2009). Mantle shear-save velocity structure beneath the Hawaiian hot spot. *Science*
775 **326.** 1388- 1390.
776 Wood B. J. and Corgne A.(2007) Trace elements and hydrogen in the Earth's transition zone and
777 lower mantle. In *Mineral Physics* (ed. G.D. Price), Treatise on Geophysics, (ed. G. Schubert).
778 Elsevier, Amsterdam, Vol. 2 pp. 63-89.
779 Wood B. J. (1995) The effect of H_2O on the 410-kilometer seismic discontinuity. *Science* **268**, 74-
780 76.
781 Wu Z. and Cohen R. E. (2006) More accurate generalized gradient approximation for solids.
782 *Physical Review* B **73**, 235116.
783 Wysession M. E., Lay T, Revenaugh J., Williams Q., Garnero E., Jeanloz R., and Kellog L. (1998)
784 The D″ discontinuity and its implications. In *The Core-Mantle Boundary Region* (eds. M.
785 Gurnis, M. E. Wysession, E. Knittl and Buffet B.) Geodyn. SerAGU, Washington, D.C., Vol, 28,
786 pp. 273–297.
787 Zindler A. and Hart S. (1986) Chemical Geodynamics. *Annual Rev. Earth Planet. Sc.* **14**, 493-571.
788

CAPTIONS OF THE FIGURES

Figure 1. $K(P,T,x)_D$ at 1500 and 2500 K, for MSWV (**a**) and MSWA (**b**).

Figure 2. MSVW, $\xi_{\omega,MSWV}/\ \xi"_{0,MSWV}$, and MSWA, $\xi_{\omega,MSWA}/\xi"_{0,MSWA}$, energy modeling. See Equ.9(a)-(b), for an explanation of ξs.

Figure 3. $K(P,T)_{D,H_2O}^{pe/pvk}$ as a function of *P*, *T* and *BWC* (Bulk Water Content), for MSWV (**a**) and MSWA (**b**). Empty and filled symbols correspond to 30 and 80 GPa, respectively. Triangles: H_2O uptake value of ≈1500 ppm; circles: H_2O uptake value of ≈800 ppm.

Figure 4. Periclase-to-perovskite H_2O-contents ratio as a function of *BWC*. LM-MSWV: filled squares/filled line; LM-MSWA: filled diamonds/filled line; BSE-MSWV: empty squares/dashed line; BSE-MSWA: empty diamonds/dashed line.

Table 1

Table 1. Lower mantle major element composition and mineral modal estimates obtained by mass balance calculations.

	BSE			LM
	*	**	#	***
wt%				
SiO_2	45.00	45.01		47.53
Al_2O_3	4.45	3.59		4.04
FeO	8.05	7.94		8.23
MgO	37.80	38.97		37.87
CaO	3.55	2.73		2.32
Mg-*Pvk*	74	76	75	78
Pe	16	16	16	14
Ca-*Pvk*	7	6	6	6
Al_2O_3-H*P*phase	3	2	3	2
	r^2=0.34	r^2=0.13		r^2=0.41

Major element mineral compositions from pyrolite-like experiments of Walter et al. (2004) and Corgne et al. (2005)
*= McDonough and Sun (1995)
**= Javoy et al. (2010)
*** = after Matas et al. (2007)
# BSE averaged mineral modal percentage used in calculation

Table 2

Table 2. Water budget estimates in mantle repositories.

	Earth Mass (gr)	BSE mass (gr)	Upper mantle	Transition zone	Lower mantle	Bulk mantle
			(Fraction of Earth total mass)			
	5.98E+27	4.00E+27	0.103	0.075	0.492	
Thickness (km)			420	300	2170	2890
H_2O (ppm)		1100-3000[1,2,3]	200-300[4,5]	1.0 -1.3 (wt%)[6, 7]	A-2000[6,8,9]	1500-2400[3,6]
Suggested value			250	1.2 (wt%)	**800/1500** **(this study)**	
					(A: value < 1000 ppm)	

1= McDonough an Sun (1995); 2=Palme and O'Neill (2004); 3= Marty (2012); 4= Dixon et al.(2002); 5= Saal et al. (2002); 6=Othani (2005); 7=Pearson et al (2014);8= Murakami et al.(2002); 9=Hernandez et al. (2013).

Table 3. *a* and ω parameters for MSWV and MSWA models. See text for their meaning.

	MSWV model	
ω_0 (kJ/mol)	ω_1 (kJ/mol/GPa)	ω_2 (kJ/mol/GPa^2)
145411.184	-4.77619218	0.0190667
a_0(kJ/mol)	a_1(kJ/mol/GPa)	a_2(kJ/mol/GPa^2)
-290293	5.7369	0.0057
	MSWA model	
ω_0 (kJ/mol)	ω_1(kJ/mol/GPa)	ω_2 (kJ/mol/GPa^2)
581384	-14.2968	0.0464
a_0(kJ/mol)	a_1(kJ/mol/GPa)	a_2(kJ/mol/GPa^2)
-290293	5.7369	0.0057

Table 4. $< {}_{BWC} K_{D,H_2O}^{pe/pvk} >$ as a function of *BWC* (ppm) for the two H-incorporation models. Bold: reference values.

MSWV		
BWC (ppm)	$< {}_{BWC} K_{D,H_2O}^{pe/pvk} >$ BSE model	$< {}_{BWC} K_{D,H_2O}^{pe/pvk} >$ LM model
100	0.987	0.988
300	0.962	0.965
800	**0.906**	**0.913**
1500	**0.836**	**0.848**
2000	0.791	0.806
2500	0.749	0.767
3000	0.711	0.731
MSWA		
BWC (ppm)	$< {}_{BWC} K_{D,H_2O}^{pe/pvk} >$ BSE model	$< {}_{BWC} K_{D,H_2O}^{pe/pvk} >$ LM model
100	0.965	0.968
300	0.899	0.908
800	**0.759**	**0.780**
1500	**0.610**	**0.638**
2000	0.529	0.559
2500	0.462	0.494
3000	0.408	0.439

Figure 1 a,b

Click here to download high resolution image

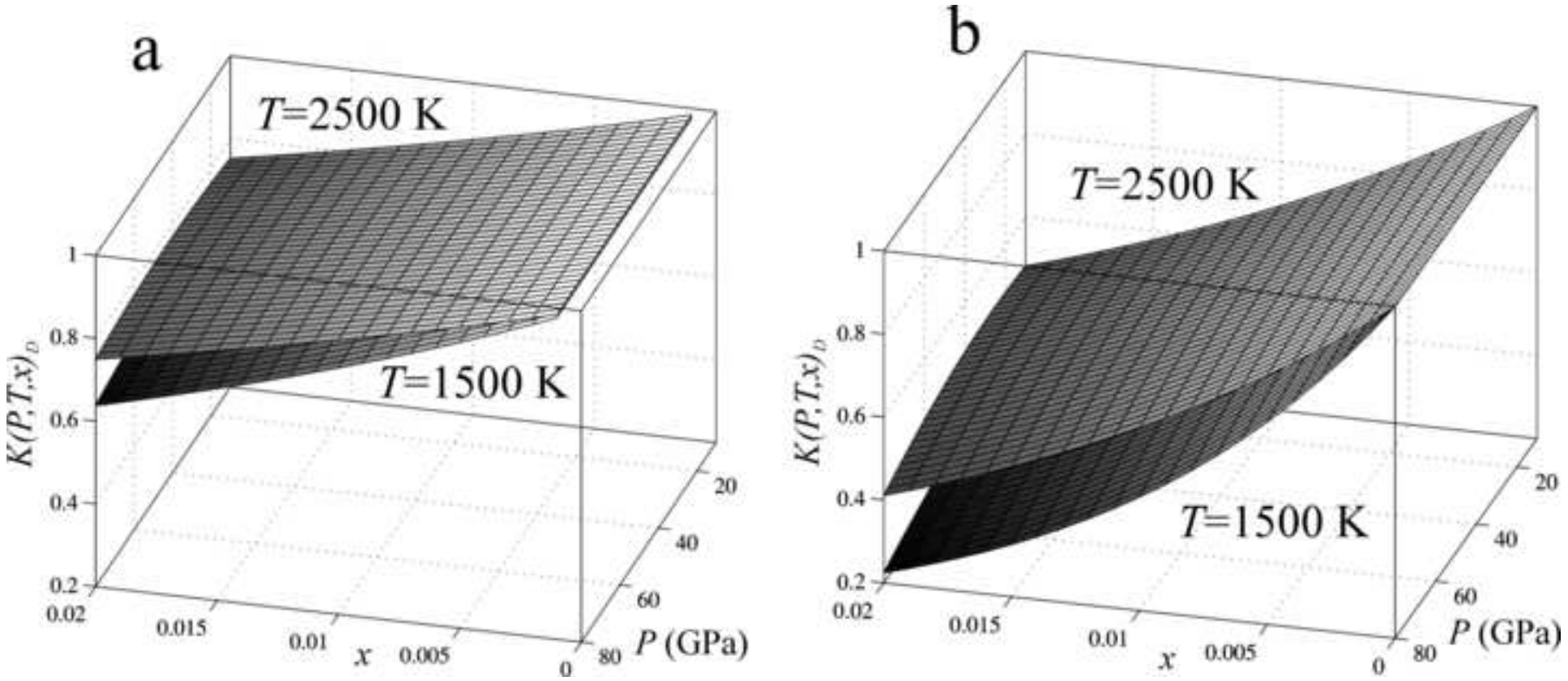

Figure 2

Click here to download high resolution image

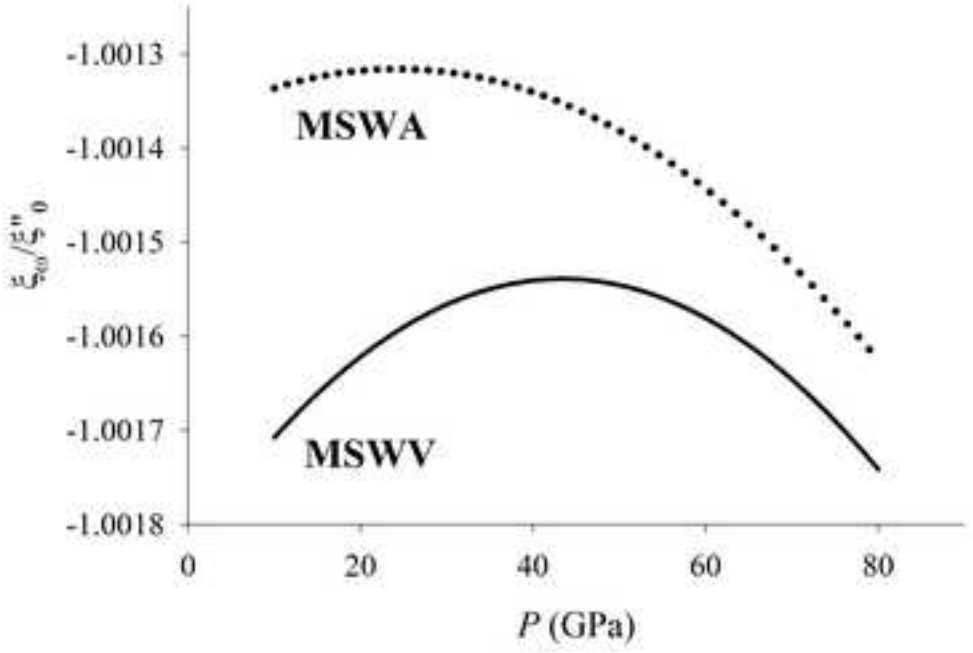

Figure 3 a,b

Click here to download high resolution image

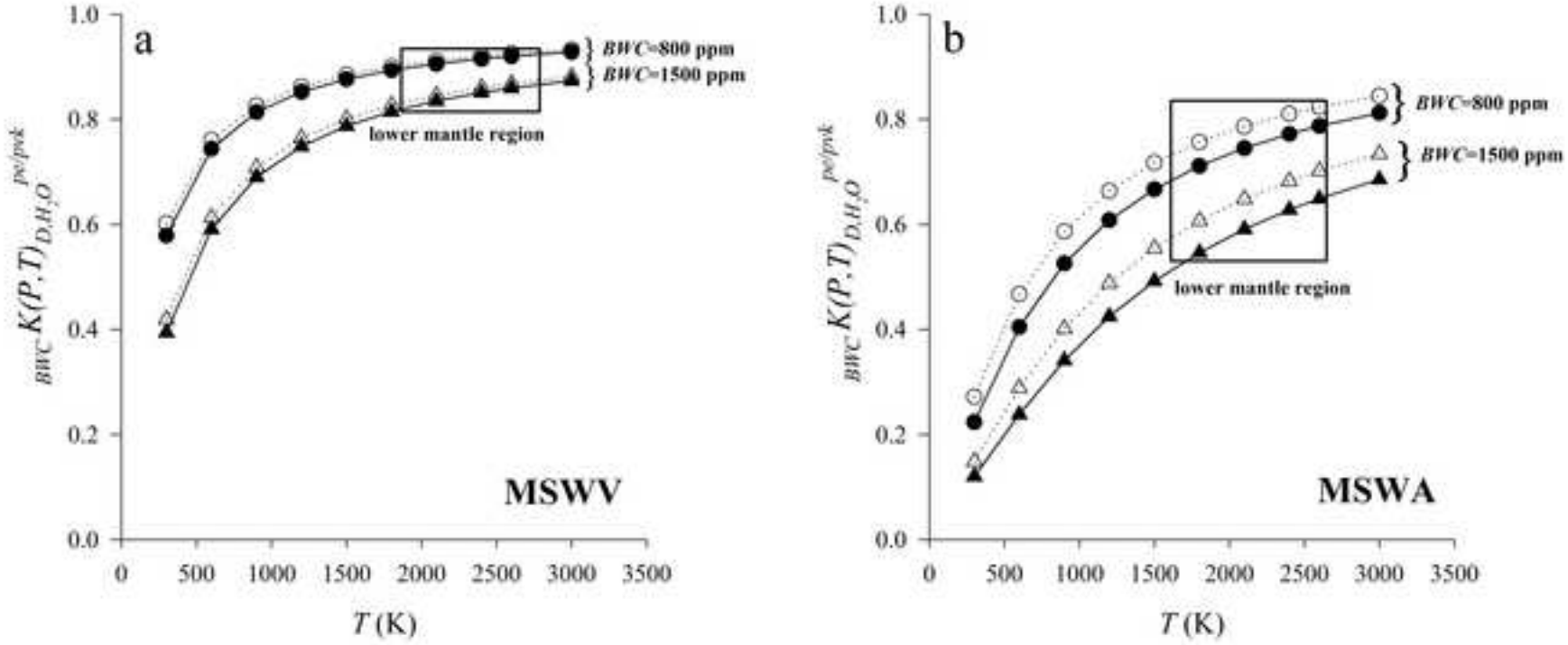

Figure 4

Click here to download high resolution image